*Tellus (2005), 57B, 124–140*
*Printed in UK. All rights reserved*



**TELLUS**

# Radon-222 in boundary layer and free tropospheric continental outflow events at three ACE-Asia sites

*By* WLODEK ZAHOROWSKI[1]*, SCOTT CHAMBERS[1], TAO WANG[2], CHANG-HEE KANG[3], ITSUSHI UNO[4], STEVEN POON[2], SUNG-NAM OH[5], SYLVESTER WERCZYNSKI[1], JIYOUNG KIM[5] and ANN HENDERSON-SELLERS[1], [1]*Australian Nuclear Science and Technology Organisation, PMB 1, Menai, NSW, 2234, Australia;* [2]*Department of Civil and Structural Engineering, The Hong Kong Polytechnic University, Kowloon, Hong Kong, China;* [3]*Department of Chemistry, Cheju National University, Ara-Dong 1, Jeju 690-756, Republic of Korea;* [4]*Research Institute for Applied Mechanics, Kyushu University, Kasuga Park 6-1, Kasuga 816-8580, Fukuoka, Japan;* [5]*Meteorological Research Institute, Sindaebang-dong, Dongjak-gu Seoul 156-720, Republic of Korea*

(Manuscript received 4 March 2004; in final form 30 August 2004)

ABSTRACT

A 1-year record of hourly atmospheric radon-222 concentration observations at three ACE-Asia network sites—Hok Tsui (Hong Kong), Gosan (Jeju Island) and Mauna Loa Observatory (Hawaii)—is presented and discussed. The observations include the spring 2001 ACE-Asia intensive operation period. Site locations were chosen for the experimental characterization of both boundary layer (Hok Tsui, Gosan) and free tropospheric (Mauna Loa) continental outflow to the Pacific. A significant seasonal variability in background radon concentration is quantified at each site with the ratios of winter maximum to summer minimum background of 96, 15 and 3 for Hok Tsui, Gosan and Mauna Loa, respectively. Only during summer were background radon concentrations directly comparable with unperturbed marine values ($\sim$20 mBq m$^{-3}$). The variability in radon signal was characterized at each site on diurnal to seasonal timescales. The seasonal variability in fetch regions for air masses experiencing the greatest and smallest terrestrial influence was characterized using 10-day back trajectories of air masses corresponding to radon concentrations higher (lower) than the 90th (10th) percentile value. The trajectory analyses for Hok Tsui and Gosan, as well as a direct analysis of the experimental results, further supports the previously postulated existence of a strong spatial heterogeneity in the radon source strength in East Asia. Back trajectories of free tropospheric air masses reaching Mauna Loa indicated source regions deep within the Asian continent primarily between 20 and 40°N. This fetch region is different from that influencing the Hok Tsui and Gosan sites. The radon concentration of air masses reaching Mauna Loa was shown to vary seasonally as well as with latitude of the predominant fetch region. Possible mechanisms of this phenomenon have been identified and include (a) seasonal variation in the radon source, (b) seasonal variation in the strength, frequency and/or efficiency of mechanisms that lift boundary layer air to the mid troposphere and (c) seasonal variation in the latitudinal axis of convection.

## 1. Introduction

### 1.1. *Background*

The atmosphere overlying the Pacific Basin is far from pristine (Nakaya et al., 1957; Bodhaine, 1983; Gao et al., 1992; Dibb et al., 1996; Board et al., 1999). Trace gases and aerosols originating from a variety of terrestrial source regions, some even with relatively short residence times, have been observed throughout much of the atmospheric column of the Pacific Basin (e.g. Balkanski et al., 1992). This is of particular interest, because some of the greatest uncertainties in current climate models can be attributed to the radiative and optical properties of aerosols (Guelle et al., 1998a; Climate Change, 2001, and references therein).

Of the various methods that have been used to investigate the frequency, intensity and spatial extent of pollution incursions to the remote Pacific atmosphere, radon ($^{222}$Rn) is unique, in that it is an unambiguous indicator of recent terrestrial influence on an air mass (e.g. Balkanski et al., 1992), irrespective of whether the region is dominated by natural or anthropogenic sources of pollutants. Air mass characterization using tracers such as radon is an integral part of determining trends in background concentrations of trace species (Perry et al., 1999; Pochanart et al., 1999).

Radon is a radioactive gaseous decay product of radium ($^{226}$Ra), which is ubiquitous in most rock and soil types. It has a

*Corresponding author.
e-mail: wza@ansto.gov.au

relatively short half-life (3.8 d), and since terrestrial radon fluxes are two to three orders of magnitude greater than oceanic fluxes (Wilkening and Clements, 1975), there is a large contrast between radon concentrations in continental and aged oceanic air masses. Radon is inert, and poorly soluble in water (Jacob and Prather, 1990; Li and Chang, 1996), so its predominant atmospheric sink is radioactive decay. Since the half-life of radon is comparable to the lifetimes of short-lived atmospheric pollutants (e.g. $NO_x$, $SO_2$), the residence times of water and aerosols and the timescale of many important aspects of atmospheric dynamics, it is a particularly useful tracer at local, regional or global scales. The radon flux from ice-free terrestrial surfaces is usually considered to be constant, and within the range 0.72–1.2 atom $cm^{-2}$ $s^{-1}$ (Turekian et al., 1977; Lambert et al., 1982). Excluding polar regions, the flux is most frequently assumed to be $\sim$1 atom $cm^{-2}$ $s^{-1}$, which is accurate to within about 25% globally (Jacob et al., 1997). There is growing evidence that latitudinal and regional gradients exist that are large enough to warrant being accounted for in regional and global simulations (Lee and Feichter, 1995; Guelle et al., 1998b; Schery and Wasiolek, 1998; Giannakopoulos et al., 1999; Conen and Robertson, 2002).

### 1.2. *Continental outflow from Asia to the Pacific*

Outflow from Asia has the most pervasive influence on the atmosphere of the Pacific Basin (Andreae et al., 1988; Merrill, 1990; Balkanski et al., 1992; Gregory et al., 1997; Perry et al., 1999). There are two pathways by which this outflow usually enters the Pacific Basin: at low levels (>700 hPa), restricted primarily to the marine boundary layer (MBL), and within the mid to upper troposphere (Kritz, 1990; Balkanski et al., 1992).

Outflow events within the MBL are closely tied to the Asian monsoonal cycle (Crawford et al., 1997; Pochanart et al., 1999). With the cessation of the summer monsoon, an anticyclone develops in the middle of the Eurasian continent and a cyclone over the northern Pacific at about 40°N (Kajii et al., 1997). Subsequently, the surface winds in Southeast Asia switch from predominantly onshore to offshore. This general flow, supplemented by the passage of fronts and other synoptic systems, can push Asian continental aerosols and trace gases into the western Pacific, sometimes as far as the Midway Islands (Balkanski et al., 1992). Compared with the upper level transport, however, this pathway to the Pacific is relatively slow.

Outflow events within the free troposphere are the result of advection within the jet stream (Merrill et al., 1989; Kritz, 1990). The mean axis of the jet stream associated with the Pacific anticyclone is 30°N (Harris and Kahl, 1990; Talbot et al., 1997), although over the year its influence is felt across a wide (20–50°N) latitude band (Gregory et al., 1997; Talbot et al., 1997). In winter and spring, when the jet stream is most intense (speeds of 60–100 m $s^{-1}$) (Talbot et al., 1997; Martin et al., 2003), air masses can reach North America in several days.

Dust is one of the most important pollutants in tropospheric outflow events. While the meteorological mechanisms to transport dust are in place from late autumn to early summer (and strongest in winter; Harris and Kahl, 1990), the optimum temporal window for dust generation is late winter to early spring, in the dry period between the thawing of winter snows and the onset of monsoonal rain (Holmes and Zoller, 1996; Talbot et al., 1997). The primary mechanisms for lifting boundary layer air into the troposphere are cold fronts (Littmann, 1991) and deep convection (Balkanski et al., 1992; Dibb et al., 1997).

Once an air mass is lifted to the mid troposphere (5–7 km), it becomes entrained within the jet stream (Merrill et al., 1989). Air masses within the northern part of the jet stream may track directly to the west coast of North America (Martin et al., 2003). Elsewhere in the jet stream, however, it is most common for the air masses to slowly subside within the subtropical anticyclone and become entrained within the southeasterly trade winds. It is not uncommon for these air masses to reach longitudes of 130°W before being turned back into the Pacific Basin (Merrill et al., 1989).

Since the height of the MBL in the vicinity of the Mauna Loa Observatory (MLO) is of the order of 2000 m (Holmes and Zoller, 1996), appropriately selected observations at MLO (3397 m above sea level) are representative of tropospheric air masses (Harris and Kahl, 1990; Perry et al., 1999). Consequently, MLO is ideally situated to observe the winter–spring peak in tropospheric outflow events. While this outflow continues throughout summer, it is restricted to <500 hPa and latitudes north of MLO (Balkanski et al., 1992).

### 1.3. *Motivation and aims*

The Aerosol Characterization Experiment in the Asian-Pacific region (ACE-Asia) is the latest in a series of initiatives of the International Global Atmospheric Chemistry (IGAC) Project aimed at reducing the uncertainties in radiative forcing by aerosols in climate models. An intensive operation period (IOP) occurred in March–May 2001, and was supplemented at selected sites by continuous observations. The Asian region is an important study region for aerosols. For centuries it has been recognized as a source of natural aerosols (Zhang, 1984; Liu, 1985), although the extent of the impact of Asian aerosols has only been realized since the 1980s (Littmann, 1991). Furthermore, anthropogenic emissions from Southeast Asia have been increasing in recent decades (Kajii et al., 1997; Martin et al., 2003), so much so that they have been identified as soon becoming the largest source region of anthropogenic pollution in the world (e.g. Perry et al., 1999). Depending on the composition of pollutants, and the nature and degree of their interaction in transit across the Pacific, the effect on the radiative and optical properties of the Pacific, and even global, atmosphere could be substantial (Bodhaine et al., 1981; Guelle et al., 1998b; Bodhaine, 1996). Based on the typical latitudinal constraints of aeolian transport mechanisms from the Asian continent (Crawford et al., 1997; Gregory et al., 1997; Talbot et al., 1997), the primary ACE-Asia study domain was restricted to the extratropical latitudes 20–50°N. Details of the observation platforms and network of sites throughout Southeast Asia are provided in the ACE-Asia overview paper (Huebert et al., 2003).

This paper reports on the results of a unique experiment where radon was recorded simultaneously at four ground stations that represent key positions within the ACE-Asia study domain. The primary goal of the experiment was to quantify contact with land of air parcels analysed at the selected stations. Both boundary layer and free tropospheric outflows were targeted. Observations made at the three Southeast Asian sites characterize the boundary layer outflow and span the latitude range of the identified study region between the regions dominated by anthropogenic emissions and those dominated by natural emissions. The third of these sites, at Sado Island, Japan, was commissioned late in 2001. While the results from Sado Island are not reported in this paper they form part of a multiyear radon experiment. The free tropospheric outflow was traced by radon recorded at MLO. The measurements discussed in this paper represent a complete year of observations (including the March–May 2001 IOP). Data collected during the IOP are available through the ACE-Asia web site (http://saga.pmel.noaa.gov/aceasia/). Data for the remainder of 2001 as well as for subsequent years, are available from the authors on request.

Since radon is relatively unsusceptible to either wet or dry atmospheric removal processes (Jacob and Prather, 1990; Kritz et al., 1993; Li and Chang, 1996; Giannakopoulos et al., 2000), observations outflow of radon at MLO provide a good indication of free tropospheric events from Asia irrespective of the lifting mechanism responsible for the initial injection of continental boundary layer air into the troposphere.

The selected sites are either coastal or island sites, hence they are ideal for observing the continental outflow to the Pacific and regional pollution sources. The sites were chosen to be collocated with as many as possible other experiments conducted on the ground within the ACE-Asia IOP.

Following a discussion of the sites, detection method and data selection techniques, the results of this study are organized as follows. Radon concentration and variability are characterized for each site on several timescales (hourly, daily, monthly and seasonally). Seasonal background radon concentrations are then established at each site. This discussion includes evidence for spatial anisotropies of the terrestrial radon source. De-seasoned radon concentration thresholds are defined for the identification of high- and low-concentration radon events, corresponding to extremes of terrestrial influence on air parcels arriving at the site. Back trajectory analysis of air masses corresponding to the high- and low-radon events is then used to identify respective fetch regions. The seasonal variability in fetch regions is discussed and compared between sites.

## 2. Methods

Three new radon detectors were installed at ground stations across the ACE-Asia study domain (Hok Tsui, Gosan and Sado Island). In addition to the new detectors, an existing radon detector at MLO has been used. This site is in the Pacific outflow region from the Asian continent, on the eastern fringe of the ACE-Asia study domain. Results from the Sado Island detector will not be reported in this paper since it was only fully operational from September 2001.

All times used in this paper are the respective local times (LT), and when reference is made to seasons they are defined as follows: winter, December to February; spring, March to May; summer, June to August; autumn, September to November.

### 2.1. Sites and surrounds

The Hok Tsui site is on the southeastern corner of Hong Kong Island at Cape D'Aguilar (22°12′N, 114°15′E). The detector is situated on a bluff, 60 m above sea level (asl), facing the South China Sea. The sample intake is 15 m above ground level (agl). This site is near the southern boundary of the ACE-Asia study domain and has previously been used to study boundary layer outflow of continental pollution to the subtropical South China Sea region (Wang et al., 1997; 2003; and references cited therein).

The Gosan site is on the western coast of Jeju Island, South Korea (33°18′N, 126°09′E), facing the Chinese mainland. The island measures approximately 73 km (east–west) and 41 km (north–south). The detector is located on a bluff, 50 m asl, and the sample intake is ∼5 m agl. This site is near the latitudinal centre of the ACE-Asia study domain and was a focal point for much of the international research effort during the first IOP (Huebert et al., 2003).

The Mauna Loa Observatory is on the northern face of the Mauna Loa volcano (19°32.3′N, 155°34.7′W), on the island of Hawaii, at an elevation of 3397 m asl. The detector's sample intake is ∼40 m agl. This site, in the central Pacific Ocean, is approximately 8000 km from the east coast of China.

### 2.2. Radon detectors: principle of operation

Radon was measured using a dual-flow loop, two-filter detector (Whittlestone and Zahorowski, 1998). At present, the two-filter detection method (Thomas and LeClare, 1970) is the best technique for low-level counting of radon in air. Other detection techniques, which rely upon the use of radon progeny as a radon proxy, necessitate concomitant assumptions regarding equilibrium, or establishing the degree of disequilibrium, of the progeny with respect to the ambient radon (Lambert et al., 1970; Larson and Hoppel, 1973).

The principle of operation is as follows. The primary flow loop draws sample air at a flow rate that is proportional to the volume of the main detector delay chamber. (The sampling flow rate is ∼40 l $min^{-1}$ at Gosan and Hok Tsui for the 750 l detectors, and ∼80 l $min^{-1}$ at Mauna Loa for the 2000 l detector.) Sample air is conditioned as it enters the detector by the first filter. This process removes aerosols as well as ambient radon and thoron progeny. Once inside the main detector delay chamber, the radon within the sample air is delayed for a sufficient time to allow a number of new progeny to be generated. These progeny are collected on the second filter (a low-impedance fine-wire mesh) as the air within the detector is rapidly recycled within the secondary flow loop. The rate at which the progeny are collected is proportional to the radon concentration. The collected progeny decay by alpha decay, which is detected using a scintillation/photomultiplier assembly.

Each detector is designed for continuous, fully automatic operation. The response time of the detectors, defined as the time to reach 50% of the maximum count rate after a step increase in radon concentration, is about 45 min. Calibration of the detectors is performed periodically by injecting radon from a calibrated radon source. The instrumental background was also evaluated before and after the reported period. The lower limit of detection (defined as the radon concentration at which there is a counting error of 30% for a 1 h count) for the Hok Tsui, Gosan and MLO detectors was 80, 90 and 40 mBq $m^{-3}$, respectively, with corresponding sensitivities to radon of 0.25, 0.21 and 0.25 counts per second (cps) per Bq $m^{-3}$.

### 2.3. *Data and selection criteria*

Each detector was controlled, and data gathered, using a combination of a data logger and personal computer. The number of counts and detector operational parameters (internal tank pressure, temperature, photomultiplier high voltage, blower status for each flow loop and logger battery voltage) were scanned at 10 s intervals, and totals/averages stored every 30 min.

Following quality control, the data were lagged to account for the instrument response time prior to aggregating to hourly counts to match meteorological data. The instrumental background count rate was then removed prior to calibration. The data recovery rates for 2001 were 89, 91 and 83% for Gosan, Hok Tsui and Mauna Loa, respectively.

It is envisaged that data from this continuing experiment will be a source of evaluation data for regional transport models. Thus, results will be presented in a way to facilitate subsequent comparisons with models. The diurnal variation of boundary layer height can exert a strong influence on trace gas concentrations measured at the surface (e.g. Ussler et al., 1994; Culf et al., 1997). Radon-derived benchmarks for evaluation of atmospheric models based on diurnal variability are only suitable for models with sufficient vertical and temporal resolution to resolve the atmospheric boundary layer (ABL). The vertical resolution of such models is usually insufficient to capture the development of the shallow nocturnal boundary layer. Since the ABL is usually well mixed, the most appropriate comparisons between observed and modelled radon concentrations are likely to be realized in the mid afternoon, when the ABL depth reaches its maximum (e.g. Jacob and Prather, 1990; Jacob et al., 1997).

In light of the above, characterization of radon concentrations on timescales greater than 1 d will be presented in two ways: (1) based on averages of all available data and (2) based on averages of diurnal minimum values. Depending upon the season, the diurnal minimum radon concentrations at the East Asian sites occurred between 13:00 and 18:00. In each case, the average of the lowest 3 hourly radon concentrations from these periods is henceforth referred to as the daily minimum radon concentration.

At MLO the daily minimum radon concentration occurs at night, and identifies the time when observations are representative of tropospheric conditions (i.e. not contaminated by local radon advected to the site by anabatic winds). A nocturnal sampling window of 22:00–07:00 was considered representative of the tropospheric radon concentration based on diurnal radon composites (see Section 3.2). Several other nocturnal sampling windows for tropospheric samples at MLO have been suggested including 00:00–07:00 (Dentener et al., 1999 for radon), 22:00–08:00 (Perry et al., 1999 for aerosols) and 00:00–08:00 (Bodhaine, 1996 also for aerosols).

### 2.4. *Selecting trajectories for fetch region analysis*

Since radon is indicative of terrestrial influence on an air mass, selecting trajectories using radon is a way of identifying (1) the primary source regions of pollution events and (2) the most appropriate sampling times to characterize the properties of the least terrestrially affected air parcels.

The monsoonal influence at the East Asian sites is shown to cause a pronounced seasonal cycle in both the mean and background radon signal (see Section 3.1). Consequently, prior to setting selection thresholds for high- and low-radon events it was necessary to remove the seasonal variability in the observed radon concentrations by removing the minimum radon concentration defined over synoptic timescales from the annual radon time-series (see Section 3.3). This seasonal variation in minimum radon concentration will henceforth be referred to as the seasonal background, and the difference between the observed concentrations and the seasonal background as the de-seasoned radon.

A database was compiled for each site containing 10-day back trajectories for every hour of 2001. Seasonal thresholds for high- and low-radon events were arbitrarily set to the 90th and 10th percentile de-seasoned radon concentrations, respectively. The database was queried for all trajectories corresponding to periods where de-seasoned radon concentrations were less (greater) than these threshold 10th (90th) percentile values. The resulting sets of trajectories corresponding to high- and low-radon events were then sampled at 3-hourly intervals for display and analysis.

The approach outlined above is but one of numerous ways that could have been used for event analysis. Balkanski et al. (1992) used a set event threshold of twice the value of the mean, Merrill et al. (1989) used an event threshold of half a standard deviation above the mean value, whilst Jaffe et al. (1997) selected events above a threshold value from a defined seasonal cycle.

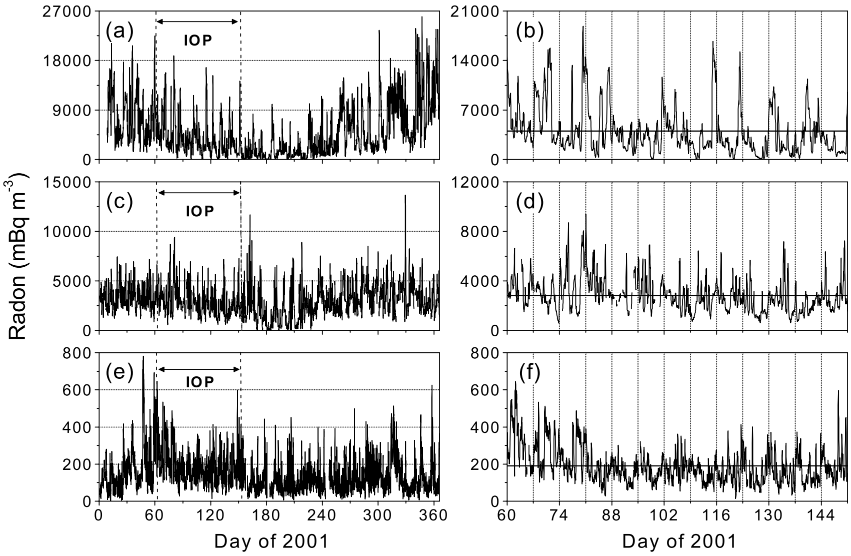


*Fig 1.* Time series of observed hourly radon concentration (mBq $m^{-3}$) for 2001, and the spring IOP, at Hok Tsui (a, b), Gosan (c, d) and Mauna Loa (e, f). The IOP mean radon concentration, and weekly intervals, are denoted by horizontal and vertical lines, respectively. Note the difference in scales.

## 3. Results

### 3.1. Annual and seasonal timescales

Mean annual radon concentrations (±1 standard deviation, $\sigma$) were 5065±$\sigma$4640, 2868±$\sigma$1511 and 146±$\sigma$97 mBq $m^{-3}$, at Hok Tsui, Gosan and Mauna Loa respectively. Corresponding hourly radon time-series are shown in Fig. 1. Weekly and monthly mean values are presented in Figs 2 and 3. Distributions (10th, 50th and 90th percentile values) of hourly radon concentration for the year and the spring IOP are shown in Table 1; monthly distributions are shown in Table 2.

The annual range of radon concentration was largest at Hok Tsui and smallest at Mauna Loa. The annual variability of radon concentration was largest at Hok Tsui and smallest at Gosan.

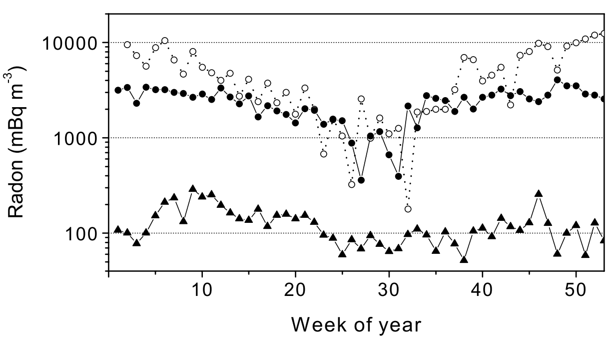


*Fig 2.* Seasonal cycle of weekly mean radon concentration for Hok Tsui (open circles), Gosan (full circles) and Mauna Loa (triangles) derived from daily minimum radon concentrations. Note the semilogarithmic scale.

These differences were largely attributed to differences in seasonal and synoptic meteorology, transport mechanisms (boundary layer versus tropospheric) and relative proximity to, and strength of, continental sources. At the East Asian sites the degree of mixing of air masses *en route* to the sites (horizontal dispersion within the boundary layer and ventilation from the boundary layer) also contributed to the variability of radon concentration.

There was a pronounced seasonal cycle of radon concentration at each site (Fig. 3). At the East Asian sites the phase of this cycle was driven by monsoonal circulation patterns. Hok Tsui radon concentrations were characterized by a winter maximum (during regional offshore flow), summer minimum (during regional onshore flow), and gradual transitions between these extremes in spring and autumn. Similar seasonal cycles of radon concentration in Southeast Asia have been reported for sites in Japan and China (Iida et al., 2000) and in India (Debaje et al., 1996). By comparison, there was no distinct winter maximum at Gosan, and the summer minimum, whilst pronounced, was quite abrupt. In fact, from October to March there was no significant difference between the monthly mean values. Prolonged oceanic events were less frequent at Gosan, with Japanese main islands enhancing radon concentrations in a large proportion of oceanic air parcels.

An examination of seasonal trends in wind direction at Gosan and Hok Tsui (Fig. 4) offers some explanation of the differences in radon cycles between the two sites. The Hok Tsui wind direction was typically between north and east (predominantly continental fetch) throughout autumn and winter, consistent with an interaction between continental outflow and trade wind circulation patterns. Starting in spring, wind direction was typically

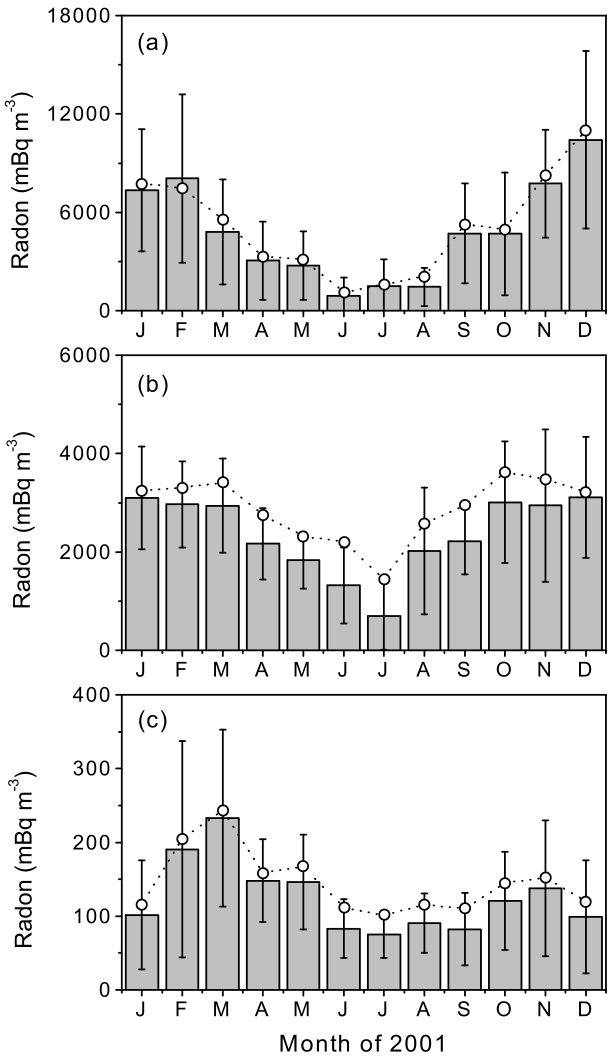


*Fig 3.* Mean monthly radon concentration at (a) Hok Tsui, (b) Gosan and (c) Mauna Loa. The open circles represent means based on all hourly data whereas the bars represent means based on daily minimum concentrations. Whiskers on bars denote ±1 standard deviation. Note the difference in scales.

between east and southwest (predominantly oceanic fetch), consistent with a strong influence of onshore monsoonal circulation patterns.

At Gosan there was a slight preference for southerly winds in summer. As indicated by the cluster of 10-day back trajectories in Fig. 5, some of the associated air masses had extensive oceanic fetch. This period coincides with the time of minimum mean monthly radon concentration. However, for the remainder of the year there was a large degree of variability in wind direction, which in part accounts for the similarity in mean monthly radon concentrations from October to March. Spring was the period of greatest variability in wind direction, consistent with the build-up to the summer monsoon.

*Table 1.* 10th, median and 90th percentile radon concentrations (mBq $m^{-3}$) at all sites for all of 2001 as well as the IOP (spring 2001)

| Radon | 2001 | | | IOP | | |
|---|---|---|---|---|---|---|
| (mBq $m^{-3}$) | 10th | Median | 90th | 10th | Median | 90th |
| Hok Tsui | 575 | 3456 | 12095 | 847 | 2949 | 9416 |
| Gosan | 1138 | 2685 | 4822 | 1354 | 2585 | 4526 |
| Mauna Loa | 51 | 122 | 273 | 92 | 170 | 326 |

At MLO, the phase of the seasonal radon cycle is driven by tropospheric transport mechanisms. Consequently, the dominant early spring peak of the cycle is out of phase with the mid-winter maximum of the East Asian sites. Radon concentrations at MLO were low in summer and winter, with two periods of enhanced radon concentration, with the main maximum in spring and a less pronounced maximum in autumn. This is because similar tropospheric transport mechanisms operate in autumn as in spring, but with less intensity (Balkanski et al., 1992; Dibb et al., 1997). Several studies targeting mineral dust and anthropogenic aerosols have identified similar seasonal cycles in the central and western Pacific (Bodhaine et al., 1981; Merrill et al., 1989; Gao et al., 1992; Holmes and Zoller, 1996; Perry et al., 1999).

The amplitudes of the seasonal cycles of radon (defined here as the difference between the highest monthly 90th percentile and the lowest monthly 10th percentile values) at Hok Tsui, Gosan and MLO are 18 776, 4828 and 360 mBq $m^{-3}$, respectively (Table 2). This large difference in amplitude can be attributed in part to relative proximity to the Asian continental source. Hok Tsui is a coastal site (close to continental sources), Gosan is an island site (relatively close to continental sources) and MLO is a remote marine site (far from continental sources). The further away a site is from a continental source, the greater the effects of air mass dilution (via horizontal mixing or vertical dilution processes) and decay of radon over the ocean. These factors combine to reduce the amplitude of annual and short-timescale variability of the radon signal. A further reduction in radon concentration applies to observations at MLO, since they are mostly representative of tropospheric radon concentrations.

However, it seems unlikely that differences in wind speed, direction, dilution and proximity to the Asian continent can completely account for the difference of 13 948 mBq $m^{-3}$ observed between the seasonal amplitudes (as defined above) of Hok Tsui and Gosan. Other factors that may have contributed to this difference include:

(1) A local (Xu et al., 1993) and/or global (Conen and Robertson, 2002) latitudinal gradient of radon flux resulting from a similar gradient in the terrestrial $^{226}$Ra content. Following an analysis of available radon flux data, Conen and Robertson (2002) came to the conclusion that there is a latitudinal gradient (decreasing northwards) in radon flux, starting from 30°N.

(2) The Asian continental radon source is affected by snow cover and freezing at higher latitudes (Dörr and Münnich, 1990).

*Table 2.* 10th, median and 90th percentile radon concentrations (mBq m$^{-3}$) at all sites for the 2001 hourly observations

| | Hok Tsui | | | Gosan | | | Mauna Loa | | |
|---|---|---|---|---|---|---|---|---|---|
| Month | 10th | Median | 90th | 10th | Median | 90th | 10th | Median | 90th |
| January | 2968 | 6394 | 13531 | 1932 | 3156 | 4662 | 37 | 98 | 218 |
| February | 2761 | 6292 | 14304 | 1932 | 3192 | 4857 | 82 | 160 | 386 |
| March | 1806 | 4296 | 12089 | 1795 | 3219 | 5326 | 125 | 213 | 400 |
| April | 755 | 2588 | 6280 | 1378 | 2606 | 4308 | 89 | 157 | 227 |
| May | 487 | 2182 | 7729 | 1177 | 2178 | 3765 | 79 | 152 | 280 |
| June | 10 | 698 | 2734 | 252 | 1798 | 4416 | 43 | 91 | 215 |
| July | 197 | 1015 | 3743 | 157 | 901 | 3973 | 40 | 78 | 200 |
| August | 40 | 1444 | 4941 | 768 | 2353 | 4491 | 53 | 106 | 179 |
| September | 1203 | 5262 | 9968 | 1706 | 2761 | 4689 | 44 | 91 | 212 |
| October | 1527 | 3154 | 11374 | 1956 | 3619 | 5290 | 62 | 131 | 246 |
| November | 2932 | 8762 | 13369 | 1427 | 3158 | 5540 | 44 | 121 | 310 |
| December | 3863 | 10574 | 18786 | 1749 | 2994 | 4985 | 44 | 88 | 257 |

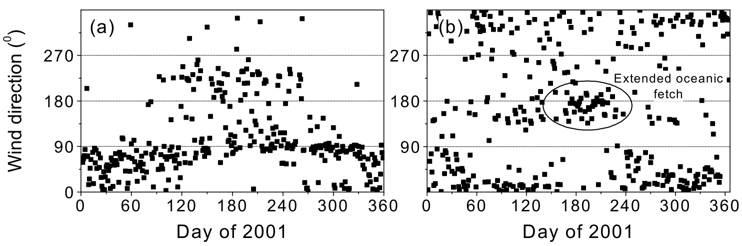


*Fig 4.* Daily (afternoon) wind direction at (a) Hok Tsui, and (b) Gosan for 2001.

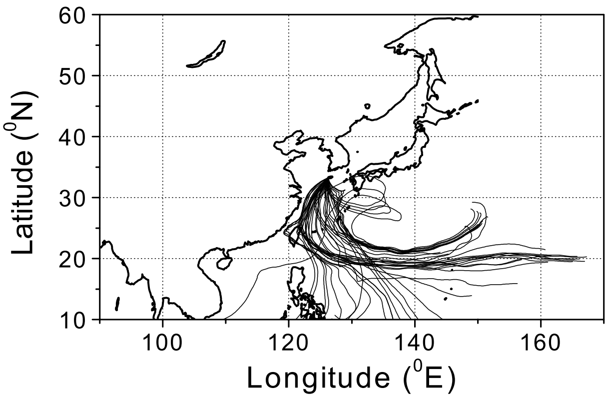


*Fig 5.* A cluster of 10-day back trajectories of air masses at Gosan corresponding to the ≤50th percentile radon concentrations between 24 June and 5 August 2001 (marked in Fig. 4 as a period of extended oceanic fetch).

(3) Specific regions of elevated radon flux that may exist within Southeast Asia. This has previously been suggested by Schery and Wasiolek (1998) and Jacob et al. (1997). Several radon studies, using a variety of measurement techniques, support the possibility that there are localized areas in mainland China with anomalously high radon fluxes (Yamanishi et al., 1991; Jin et al., 1998; Iida et al., 2000). The location of areas with enhanced radon fluxes ranges from northwest to northeast of Hok Tsui, some just over 500 km away (see also the discussion of predominant fetch areas in Section 4.2).

The lack of direct flux measurements in the Southeast Asian region makes it difficult to evaluate the relative contribution of these factors to the differences observed between Hok Tsui and Gosan.

Synoptic meteorological conditions also have a pronounced effect on the observed radon concentrations at the East Asian sites. Most of the high-frequency variability superimposed on the annual radon cycles of Hok Tsui and Gosan is a result of short-term changes in fetch region brought about by synoptic events. For instance, in spring the passage of synoptic systems is more regular, and their effect on observed radon concentrations more pronounced at Hok Tsui than at Gosan (Figs 1b and d). Radon events above or below the spring mean radon concentration are typically of longer duration at Hok Tsui than at Gosan. The varying duration of radon events is a measure of persistence of air masses representing a fetch region. Furthermore, the comparatively lower amplitude of these events from the mean at Gosan indicates a poorer distinction between predominantly continental and marine air masses at this site.

The differences in radon concentrations observed both on seasonal and synoptic timescales between Hok Tsui and Gosan point to either stagnation of air masses in the vicinity of Gosan, or local recirculation leading to a homogenization of radon

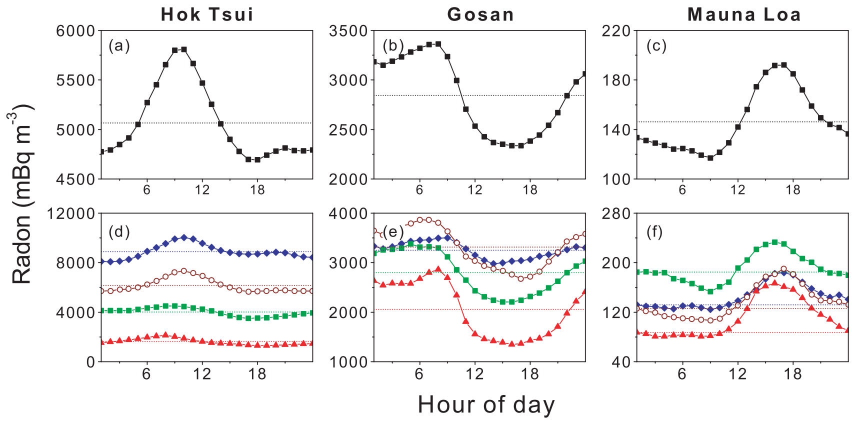


*Fig 6.* (a–c) Annual and (d–f) seasonal composite diurnal radon concentration (mBq $m^{-3}$) at Hok Tsui, Gosan and Mauna Loa for 2001. For the seasonal plots the diamonds, squares, triangles and circles represent winter, spring, summer and autumn, respectively. Horizontal dotted lines represent the respective mean concentrations.

concentrations. It is pertinent to note in this context that Akimoto et al. (1996) reported the occurrence of stationary fronts in the Gosan region. The peculiarities of local Gosan transport patterns are addressed further in the trajectory analysis of Section 4.2.

### 3.2. *Characterization of the diurnal cycle*

Diurnal composites of radon concentration at Hok Tsui, Gosan and MLO were calculated using the annual dataset (Figs 6a, b and c). All sites exhibit a clear diurnal cycle of radon concentration. At the East Asian sites this cycle is characterized by a morning maximum and afternoon minimum (between 13:00 and 18:00), whereas at MLO the converse is true.

The change in phase of the diurnal cycle at MLO is caused by the location of the site. Anabatic (up-slope) winds affect the site during the day, and katabatic (down-slope) winds affect the site by night (Mendonca, 1969). Consequently, night-time observations (lower radon concentrations) are representative of the troposphere within approximately 1 km above the site (Perry et al., 1999), whereas day-time observations are strongly influenced by the local island signature.

While the pattern of the Gosan diurnal cycle was similar to that observed inland at a site near Tokyo (Hattori and Ichiji, 1998), the amplitude was less than half that observed at the inland site (2560 mBq $m^{-3}$). The smaller diurnal amplitude at Gosan can be largely attributed to the strong marine influence on boundary layer depth at island sites (Iida et al., 2000).

Diurnal composite plots were also prepared by season (Figs 6d–f). Without exception, the diurnal changes in radon concentration were most significant in summer, and least significant in winter/spring (Table 3). Irrespective of site or season, the amplitude of the diurnal cycle of radon concentration never exceeded 2000 mBq $m^{-3}$. At the East Asian sites (i.e. within the ABL), the difference between daily mean, and daily minimum radon concentrations did not exceed 900 mBq $m^{-3}$.

Tropospheric radon concentrations at MLO (22:00–07:00) indicate that the largest and smallest terrestrial influences on tropospheric air masses occur in spring and summer, respectively.

*Table 3.* Amplitude of the diurnal cycle of radon at Hok Tsui, Gosan and Mauna Loa, and ratio of amplitude to the corresponding mean radon concentration

| | Amplitude of diurnal cycle (mBq $m^{-3}$) | | | Ratio of diurnal amplitude to mean concentration | | |
|---|---|---|---|---|---|---|
| | Hok Tsui | Gosan | Mauna Loa | Hok Tsui | Gosan | Mauna Loa |
| 2001 | 1113 | 1027 | 75 | 0.22 | 0.36 | 0.51 |
| Winter | 1961 | 524 | 60 | 0.22 | 0.16 | 0.45 |
| Spring | 989 | 1176 | 80 | 0.25 | 0.42 | 0.43 |
| Summer | 852 | 1517 | 86 | 0.53 | 0.74 | 0.98 |
| Autumn | 1673 | 1185 | 84 | 0.27 | 0.36 | 0.67 |

In spring, and to a lesser extent in autumn, radon concentrations within the nocturnal sampling window continue to decrease until sunrise. Assuming that this period is representative of tropospheric radon concentrations, and that katabatic drainage flows increase in strength until sunrise as the surface continues to cool, air from progressively deeper within the troposphere will be drawn to the observatory. Thus, these observations indicate that the vertical distribution of tropospheric radon above MLO is more uniform in summer and winter than in spring and autumn.

### 3.3. *Characterization of the background radon concentration*

To establish the degree of interaction of an air mass with terrestrial sources using radon it is necessary to characterize the background radon concentration curve above which suitable event thresholds can be set. At some sites the background concentration is equivalent to the marine baseline value, which is relatively consistent all year round. However, at Hok Tsui and Gosan, where the seasonal meteorology only enables extended oceanic fetch for a limited period of the year, the background radon concentration shows a pronounced seasonality.

Before the seasonal background can be characterized, it is necessary to identify the subseasonal timeframe at which the most significant variability in radon concentration occurs. The passage of fronts and other synoptic features can strongly influence

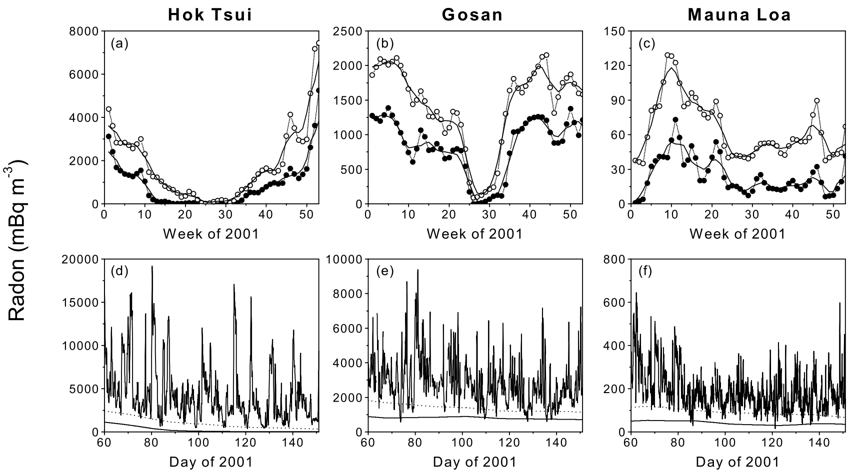


*Fig 7.* (a–c) Fortnightly minimum (full circles) and 10th percentile (open circles) radon concentration (mBq m$^{-3}$) and 5-week running mean fits for Hok Tsui, Gosan and Mauna Loa, and (d–f) fortnightly minimum (solid) and 10th percentile (dotted) curves superimposed on hourly radon concentration observations at Hok Tsui, Gosan and Mauna Loa during the IOP.

short-term trace gas observations (e.g. Kajii et al., 1997; Wang et al., 1997, 2003). In the case of coastal sites in particular, synoptically driven changes in fetch region cause variations in radon concentration that far exceed diurnal changes. Power spectral analysis of the radon and mean sea level pressure data at the sites (not shown) indicated synoptic influences of 3–14 d duration. Thus the seasonal background was constructed from fortnightly radon minima.

In the summer months, radon concentrations between the seasonal background and 10th percentile radon concentration were often representative of what is considered to be marine baseline conditions. Over this period, the minimum smoothed fortnightly 10th percentile radon concentrations were 69, 140 and 37 mBq m$^{-3}$ at Hok Tsui, Gosan and MLO, respectively. Values of the fortnightly minimum and 10th percentile radon concentrations were calculated for each site (Figs 7a–c). Smoothed minimum and 10th percentile curves are shown in Figs 7d–f superimposed on the hourly radon concentrations in the IOP. There is a mismatch evident between the December and January background radon concentrations at Hok Tsui in Fig. 7a. This mismatch is expected to diminish, or disappear, as the size of the data set increases.

The variability in seasonal background at each site closely follows the seasonal mean radon concentration, and is largely attributable to the fact that seasonal rather than synoptic meteorological patterns determine predominant fetch regions on annual timescales. This is in marked contrast to baseline stations such as Cape Grim, Tasmania (40°41′S, 144°41′E), where there is a much more even distribution of main fetch regions from month to month. As a result, the Cape Grim baseline radon concentration does not depend much on season: the winter/summer ratio of median baseline radon concentrations determined for the Cape Grim oceanic fetch was 57/43 mBq m$^{-3}$. Also, at any time, a baseline event at Cape Grim longer than about 6 h results in radon concentrations reaching levels lower than 100 mBq m$^{-3}$ (Zahorowski and Whittlestone, 1999). Hence, at this site it is possible to select a single threshold radon concentration to identify baseline (oceanic) and non-baseline events, irrespective of season, which is 100 mBq m$^{-3}$ (Gras and Whittlestone, 1992).

While the change in seasonal background at Hok Tsui was relatively gradual throughout the year, there was a sharp decrease in the background value at Gosan to the summer minimum (Fig. 7b). This decrease is associated with a cluster of southerly wind directions for this time of year, as shown in Fig. 4b. Figure 5 shows a cluster of 10-day back trajectories for air masses associated with radon concentrations below the 50th percentile value between 24 June and 5 August 2001. The back trajectories indicate that most of these air masses originate from the western Pacific and pass through the East China Sea *en route* to Gosan.

In winter, and to a lesser extent other times of the year, when outflow within the ABL is primarily offshore, the radon concentration of marine air masses 2000–4000 km off the East Asian coastline is considerably enhanced. An example of the magnitude and extent of this enhancement is provided by the radon transect of the RV *Ron Brown* from Hawaii to the Asian continent measured during the IOP (Johnson, 2001). This transect shows that radon concentration minima based on a 5-day running mean rise from 150 mBq m$^{-3}$ near Hawaii, to about 1000 mBq m$^{-3}$ in the area closest to Gosan. The latter value corresponds very well to the respective seasonal background derived from the Gosan radon data (Fig. 7b).

## 4. Characterization of air mass fetch regions

The ability to reliably characterize air mass fetch regions is of critical importance to the thorough interpretation of aerosol and trace gas samples collected at any site. Under certain circumstances, the direction of approach of air masses to the site may

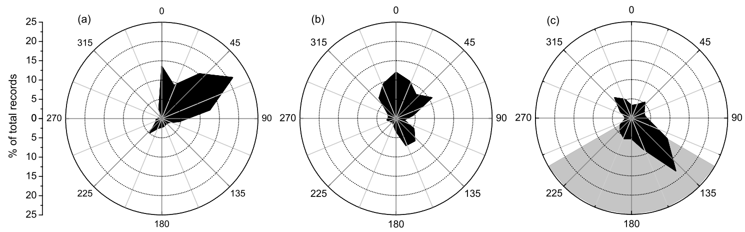


*Fig 8.* Angular distribution of number of hourly samples (as a percentage of the yearly total) based on wind direction at (a) Hok Tsui, (b) Gosan and (c) Mauna Loa for 2001. The shaded sector indicates wind directions observed during the nocturnal sampling window.

be indicative of the fetch region. The angular distribution of the number of hourly samples collected in 2001 at the three ACE-Asia sites is strongly anisotropic (Fig. 8). At Hok Tsui, there is a distinct preference for air masses to approach the site from the northeast, which is a result of interaction between monsoonal flow and trade-wind circulation near the surface in this region. At Gosan, clusters from the north and southeast confirm a monsoonal influence at this site. At MLO wind directions have a pronounced southerly component, largely attributable to nocturnal katabatic drainage winds (Mendonca, 1969).

### 4.1. Evaluation of sector analysis

While examination of the angular distribution of atmospheric constituents by sector can be used as a rough indication of fetch regions, the suitability of this technique depends on local topography and typical synoptic meteorological patterns. For coastal and island sites that satisfy the criteria for the application of sector analysis, radon is an ideal tracer to use due to the large contrast between oceanic and terrestrial radon sources (Wilkening and Clements, 1975; Schery et al., 1989). At some sites, however, as is the case for MLO, sector analysis does not provide a meaningful link to fetch areas so an alternative approach such as back trajectory analysis needs to be applied (Harris and Kahl, 1990).

To determine whether sector analysis could be used as a preliminary indicator of fetch regions for the East Asian sites, angular distributions of radon concentration were generated (Figs 9a and b). At Hok Tsui sector analysis reflects the distribution of continental and oceanic fetch quite reliably. Excluding the poorly represented northwestern sector, the maximum radon concentrations are observed from mainland China, secondary peaks to the northeast and southwest correspond to Taiwan/Japan and Hainan Island/Indochina Peninsula, respectively, and the minimum radon concentrations are observed between 100 and 210°, the oceanic sector. This indicates that wind direction can be used as a preliminary indicator of air mass origin at Hok Tsui. At Gosan, however, the angular distribution of radon shows little structure. The only significant deviation from a rather homogeneous distribution occurs for the southern sector, 180°. The relatively homogeneous angular distribution of radon implies that wind direction is not a good indication of air mass fetch region at Gosan.

### 4.2. Back trajectory fetch region analysis

Limitations in the accuracy of archived gridded meteorological data, and information about subgrid scale processes, are among the potential sources of error in trajectory simulations (Merrill, 1996). With these uncertainties in mind, a trajectory should be viewed only as a general indication of the air mass pathway, rather than a definitive depiction of reality (Harris and Kahl, 1990). Furthermore, the fact that a trajectory passes over land is no guarantee that the air mass has experienced significant terrestrial influence. Such uncertainties highlight the value of performing simultaneous tracer analysis using radon, since it is an unequivocal indicator of recent terrestrial influence.

Ten-day back trajectories were calculated using the PC version of NOAA Air Resources Laboratory's (ARL) HYbrid Single-Particle Lagrangian Integrated Trajectory (HYSPLIT) model, version 4.6 (Draxler and Hess, 1998). The model uses previously gridded meteorological data. Profiles of the meteorological data at each horizontal grid point are linearly interpolated to a terrain-following coordinate system. If the gridded meteorological data do not contain a vertical motion field, HYSPLIT calculates this field. The scalar vertical mixing coefficient is assumed to follow the coefficient for heat. Time interpolation of the meteorological fields is directly incorporated into the advection algorithm.

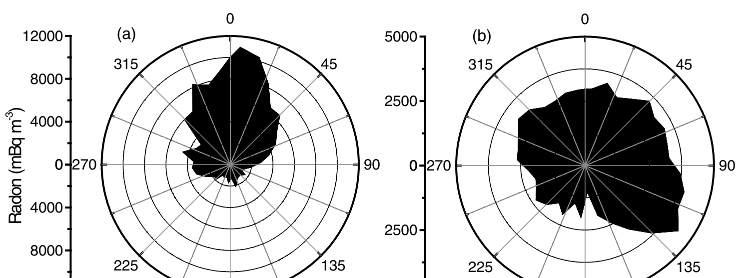


*Fig 9.* Angular distribution of daily minimum radon concentration (mBq $m^{-3}$) at (a) Hok Tsui and (b) Gosan for 2001.

Trajectories are terminated if they exit the model top, but advection continues along the surface if trajectories intersect the ground. HYSPLIT has a total of 20 vertical layers spanning the range 10–11 500 m above mean sea level (Draxler and Hess, 1997).

The meteorological data used for the back trajectory analysis in this study were the ARL FNL data archives, which consist of output from the National Weather Service National Center for Environmental Prediction's (NCEP) Medium Range Forecast model converted from a 1° × 1° grid to hemispheric 129 × 129 polar stereographic grids. All simulations were set to terminate at the elevation of observations at each site (60, 50 and 3400 m asl for Hok Tsui, Gosan and MLO, respectively).

Trajectories were used to characterize seasonal changes in fetch region(s) responsible for the high- and low-radon events (as defined in Section 2.4). To a first approximation, these categories of events relate to extremes of terrestrial influence on the sampled air mass over its recent (<10 d) history. The following discussions of results from each of the three sites are structured similarly: (1) the fetch regions for high- and low-radon events during spring (the IOP) are identified and (2) the fetch regions for the seasonal extremes of radon concentration (summer and winter) are identified and compared with those in spring.

*4.2.1. Hok Tsui.* Back trajectories for air masses corresponding to low- and high-radon events at Hok Tsui in spring are presented in Figs 10a and b. During this period, air masses corresponding to low-radon events could be separated into two main categories: those approaching the site from the south and those approaching the site from the east. Air masses approaching from the south had spent most of the previous 10 d over either the South China Sea or the western Pacific Ocean. Those approaching from the east had spent most of the previous 10 d over the East China Sea, in some cases having traversed the Asian continent at high latitudes, much of which may have still been snow-covered at this time of year, and thus the radon source suppressed. Nearly all air masses with high radon concentrations in spring approached the site from the northeast, having passed over eastern China (Fujian and Jiangxi provinces).

Back trajectories for the summer low-radon events, and winter high-radon events are presented in Figs 10c and d. The primary difference between spring and summer in fetch region for the low-radon events was that in summer very few air masses originated in the East China Sea. While some of the summer low-radon events originated from the western Pacific, most were from the South China Sea. The fetch region for winter high-radon events was similar to that for spring high-radon events, though much more consistent. The corresponding air masses approached the site exclusively from the northeast through a relatively narrow corridor, roughly along the border between the Fujian and Jiangxi provinces. Without exception, in the 10 d prior to arriving at Hok Tsui air masses corresponding to the winter high-radon events travelled southeast over Mongolia before turning south-southwest (at ~40°N) to track over eastern China.

Back trajectories for the winter low-radon events (not shown) demonstrated many similarities to the winter high-radon events (Fig. 10d). Air masses associated with these events also tracked southeast across Mongolia before turning south-southwest toward Hok Tsui, approaching via a relatively narrow corridor. The key difference was that the turning point was further south and east, near Jeju Island (~33°N, 127°E). This resulted in the trajectories hugging the eastern side of the Chinese coastline until reaching Hok Tsui. The narrow approach paths of both the

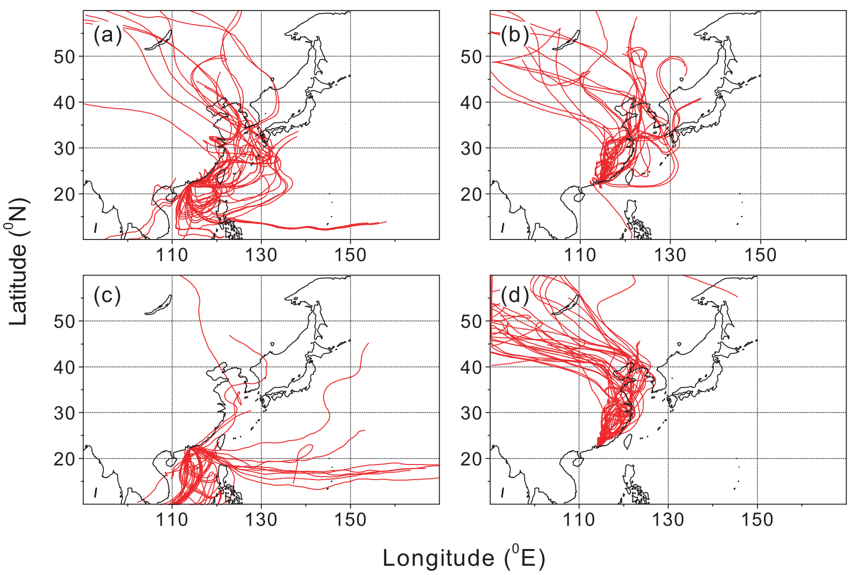


*Fig 10.* Ten-day back trajectories for air masses arriving at Hok Tsui corresponding to (a) IOP low-radon events, (b) IOP high-radon events, (c) summer low-radon events and (d) winter high-radon events.

high and low winter events may be at least partly due to the presence of a mountain range along the eastern Chinese coastline, oriented northeast/southwest with frequent peaks to 2000 m asl.

Back trajectories for the summer high-radon events (not shown) indicated no consistent direction of approach to the site. However, all air masses corresponding to the observed events had a predominantly oceanic fetch over a wide quadrant, ranging from the northeast (Kyushu, Japan) to the south-southwest (coast of Vietnam). In each case, there was a brief irregular crossing of the Chinese coastline immediately prior to arrival at Hok Tsui.

*4.2.2. Gosan.* Back trajectories for air masses corresponding to low- and high-radon events at Gosan in spring are presented in Figs 11a and b. During this period, trajectories of air masses corresponding to low-radon events indicated no preferred direction of approach to the site, nor a consistent fetch region. Clusters of trajectories representing low-radon events originated from the Sea of Japan, the Pacific Ocean south of Japan, the Yellow and East China Seas, as well as across the Asian continent traversing Mongolia and northern China. Trajectories for air masses corresponding to spring high-radon events at Gosan showed air masses approaching the site from all directions but south. While the majority of the associated air mass trajectories traversed Mongolia and northern China, few approach Gosan directly. Some pass into the Sea of Japan and get funnelled to the site through the Korea Strait, although most appear to dwell for some time above the Yellow Sea or a narrow stretch of lowlands immediately to the west of the Yellow Sea.

The frequent pooling and/or mixing of air masses in the Yellow Sea region is largely responsible for the unsuitability of the sector analysis technique (Fig. 9b), and low-amplitude seasonal variability of radon concentration at Gosan (Fig. 3). In summer and autumn, stationary fronts frequently occur between Japan and China, south of Jeju Island, at 30–32°N. Following observations in autumn 1991, Akimoto et al. (1996) described the influence of such stationary fronts on the transport of pollutants from the Asian continent.

Observations by Iida et al. (2000) indicate that the Beijing area, roughly 1000 km northwest of Gosan across the Yellow Sea, has a mean annual radon concentration of 7 Bq $m^{-3}$. Whilst trajectory analysis has indicated that many air masses *en route* to Gosan, pass over or at least near Beijing (Fig. 11), mean annual radon concentration at Gosan is only 2.9 Bq $m^{-3}$. Given the half-life of radon, this is further evidence that air masses are either substantially delayed, horizontally dispersed or vertically diluted (via boundary layer venting) in transit across the Yellow Sea.

Back trajectories for summer low-radon events at Gosan (Fig. 11c) indicate that most of the air masses originate from over the East China Sea or the Pacific Ocean. Back trajectories for winter high-radon events (Fig. 11d) show that this fetch region is also clearly defined. Most commonly, the air masses responsible for these events originate in Russia, pass over Mongolia and/or North China, before moving down the western side of the Korean Peninsula to arrive at Gosan. No air masses showing evidence of substantial terrestrial influence reach Gosan from latitudes <30°N on the Asian continent. Consequently, the Gosan site is best suited for investigating anthropogenic pollution events from northeast China or the Korean Peninsula.

The back trajectories of low summer and high winter radon events from both Hok Tsui and Gosan provide clear examples of the onshore and continental outflow phases of the Asian monsoons. As well as noting the monsoonal influence on regional transport, observations by Pochanart et al. (1999) at Oki Island

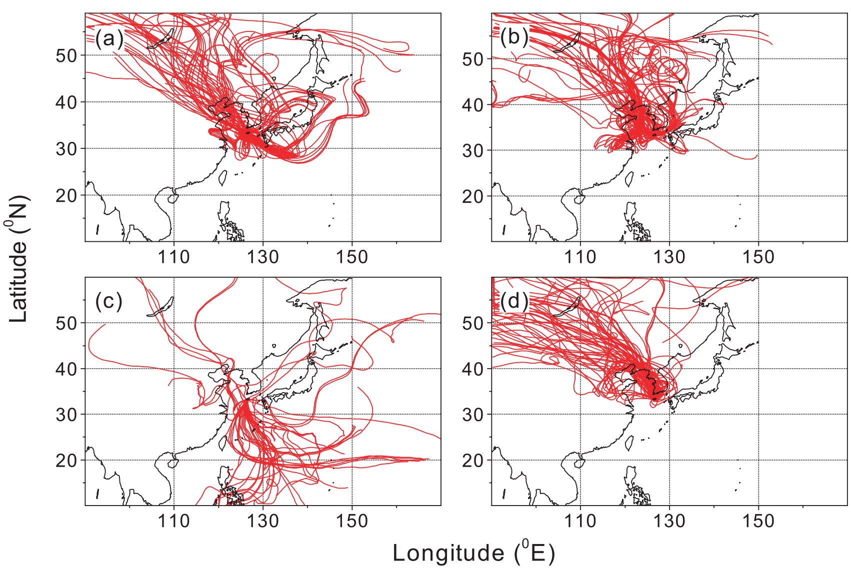


*Fig 11.* Ten-day back trajectories for air masses arriving at Gosan corresponding to (a) IOP low-radon events, (b) IOP high-radon events, (c) summer low-radon events and (d) winter high-radon events.

(700 km northeast of Gosan) indicate that the region is influenced by continental outflow for well over half of the year. Gosan fortnightly minimum radon concentrations (Fig. 7b) also indicate a relatively narrow window of low-radon events in summer. Trajectories corresponding to the low-radon events for this period only (Fig. 5) indicate quite a consistent fetch region.

Back trajectories for Gosan summer high-radon events (not shown) indicated no consistent fetch region. Most of the air masses had predominantly oceanic origins, but had experienced brief encounters with either Japan or Taiwan. The Gosan winter low-radon events (not shown) originated exclusively from the Asian continent (>40°N), as was the case for the Gosan winter high-radon events. While some of the air masses corresponding to these events were delayed for longer periods over the Yellow Sea or the Sea of Japan than was the case for the high events, it is likely that a greater proportion of their trajectories over the continent were at high altitude, though this has yet to be fully investigated.

Excluding the time spent along the Korean Peninsula, the fetch region of Gosan winter high-radon events is similar to the northern half of the fetch region for the corresponding Hok Tsui events. Given the similarities evident in much of their trajectory paths, the large difference in high-radon events observed at Hok Tsui and Gosan is indicative of a larger than usual radon source in the East China region including, though not necessarily limited to, the fetch region indicated by Fig. 10d. This fetch region covers a portion of southeastern China identified by Schery and Wasiolek (1998) as having above average surface $^{226}$Ra concentrations and radon fluxes. Also, Conen and Robertson (2002) describe a latitudinal gradient in terrestrial radon flux, decreasing north of 30°N, although based on this model the decrease in radon flux between the latitude of Hok Tsui and Gosan would be less than 10%. Furthermore, simulations by Guelle et al. (1998b) and Giannakopoulos et al. (1999) indicated that the typically assumed radon source strength underestimated the actual source strength in east Asia.

*4.2.3. Mauna Loa.* Back trajectories from MLO for low- and high-radon events in spring are presented in Figs 12a and b. Events were selected as for the Hok Tsui and Gosan sites with the additional restriction that all data outside the nocturnal sampling window (22:00–07:00) were excluded (see Section 2.3).

Back trajectories associated with MLO spring low-radon events tended to originate from the western Pacific, but showed little preference for direction of final approach to the site. With the exception of a few events that originated from the eastern fringes of the Asian continent, the fetch region of these events encompassed most of the Northern Hemisphere Pacific Basin. By comparison, the majority of the MLO spring high-radon events had fetch regions deep within the Asian continent between 20 and 40°N.

Back trajectories of air masses associated with MLO summer low-radon events (Fig. 12c) also indicated little preference for direction of approach to the site. However, compared with spring, the fetch region of summer low-radon events was mostly restricted to the eastern Pacific. In fact, none of the trajectories analysed for summer low-radon events reached a coastline on either side of the Pacific. Most of the associated air masses originated only 1000–2000 km from MLO, a characteristic that is attributable to either anticyclonically looped paths and/or low wind speeds. By comparison, the MLO winter high-radon events (Fig. 12d) originated exclusively from the west, and the corresponding air masses travelled large distances. These air masses exhibited fetch regions deep within the Asian continent, as was the case in spring, although the winter high-radon event fetch region spanned a greater latitude range within the continent (15–50°N).

Back trajectories of air masses associated with MLO summer high-radon events mostly originated from the east (not shown), either over the ocean close to the western coast of the United States or over land in California and Mexico. A few of the events originated from the far North Pacific near the Aleutian Islands. Transport to regions of the Pacific near MLO from

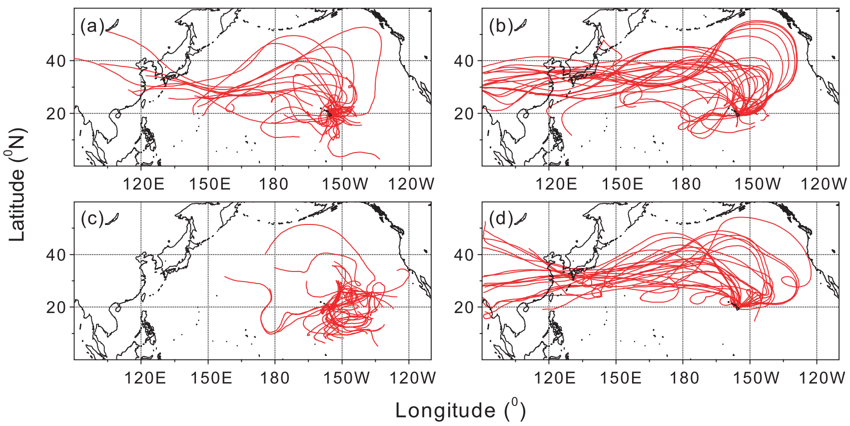


*Fig 12.* Ten-day back trajectories for air masses arriving at MLO corresponding to (a) IOP low-radon events, (b) IOP high-radon events, (c) summer low-radon events and (d) winter high-radon events.

polar regions has also been noted by Balkanski et al. (1992) and Harris and Kahl (1990). Most of the air masses associated with MLO winter low-radon events originated from the western Pacific. Some of the trajectories loop out far into the eastern Pacific (to 120–130°E) prior to arriving at MLO. Roughly 20% of these trajectories had contact with the Asian continent. The fetch regions differed from the winter high-radon events in that the air masses originated from southern Asia (∼20°N), or from the Indian Ocean, passing over Laos and southern Taiwan, *en route* to the western Pacific. The typical approach path of these air masses to MLO was also further to the south (20–25°N) than that of the air masses of the winter high-radon events (30–40°N).

*4.2.4. Analysis of MLO continental fetch.* The preceding analysis indicates some variability in the radon source with fetch region latitude in Asia. Thus an attempt was made to identify the variability in radon source by fetch region in Asia, and characterize any seasonal variability. To minimize the likelihood of local influences on the radon signal, trajectories were calculated only at 00:00, 03:00 and 06:00 each day, for the entire year. Three latitude bins were defined (20–30°N, 30–40°N and 40–50°N) to span the primary band of tropospheric outflow from the Asian continent to the Pacific (20–50°N; Crawford et al. (1997); Gregory et al. (1997); Talbot et al. (1997)). Trajectories were grouped by the latitude band within which they crossed the Asian coastline, and by season. The underlying assumption was that trajectories that cross the coast within this band remain within the band whilst over the continent. This assumption was often, but not always, true, with the fewest exceptions to the rule occurring in spring. An example of the band 30–40°N spring trajectories is presented in Fig. 13.

The distribution of radon concentrations (10th, 50th, 90th percentiles) corresponding to the selected trajectories was calculated for each latitude band and season that was sufficiently well represented (Fig. 14). Based on the categories defined above, fewer than 1% of the selected trajectories over the year fell within the 40–50°N bin. Furthermore, none of the available trajectories crossed the Asian coastline during summer 2001. Consequently, analysis was only performed for winter, spring and autumn for the 20–30°N and 30–40°N latitude bins. In each case, radon concentrations were corrected for decay over the ocean, with the assumption of zero radon input from below whilst the air mass was over the ocean.

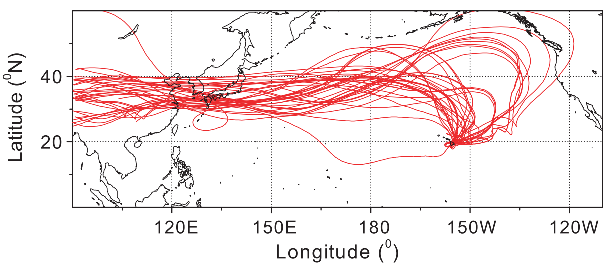


*Fig 13.* Ten-day back trajectories in spring for air masses arriving at Mauna Loa within the nocturnal sampling window that crossed the Asian coastline within the latitude band 30–40°N.

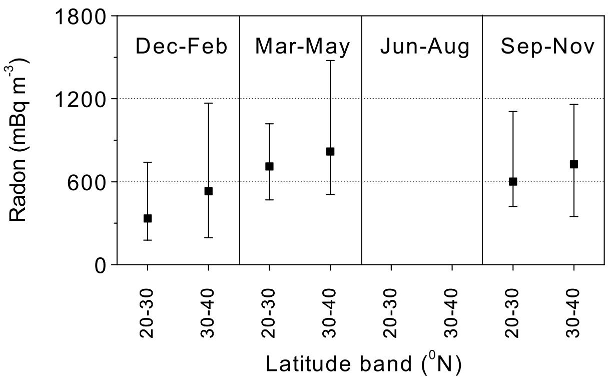


*Fig 14.* The distributions (10th, 50th and 90th percentiles) of radon concentration (mBq m$^{-3}$) by season of air masses arriving at Mauna Loa within the nocturnal sampling window that crossed the Asian coastline in the latitude band 20–30°N or 30–40°N. There were insufficient data in summer. Radon concentrations were corrected for decay over the ocean.

The most notable feature of Fig. 14 is the observed seasonality in radon concentration. Within both latitude bins the lowest concentrations are observed in winter and the highest in spring. This is in agreement with other studies that have identified spring as a time of peak transport from the Asian continent to the Pacific (Merrill et al., 1989; Balkanski et al., 1992; Crawford et al., 1997; Jaffe et al., 1997). There are at least four factors contributing to these observations:

(1) Seasonal variation in the radon source (driven by soil moisture and or snow cover, both of which inhibit radon flux; Schery and Wasiolek, 1998).

(2) Seasonal variation in the strength, frequency and/or efficiency of mechanisms that lift boundary layer air to the mid troposphere (cold fronts and wet/dry convection; Merrill et al., 1989).

(3) Seasonal variation in the latitudinal axis of convection (Dibb et al., 1997).

(4) Seasonal variation in the speed of transport across the continent from source region to the coast (Talbot et al., 1997).

Another feature of Fig. 14 is that radon concentrations from the higher latitude band are consistently greater than those from the lower latitude band. This latitudinal gradient in radon concentration is opposite in direction to that observed between the coastal ground station sites. According to Conen and Robertson (2002) there should be a decrease in radon source strength from 20–30°N to 30–40°N of between 10–20%. A possible interpretation of our findings is that injection of boundary layer air to the troposphere is more frequent or intense in the 30–40°N latitude band compared with the 20–30°N band. The two mechanisms for injection are frontal activity and convective activity. Dibb et al.

(1997) mention that there is a northward migration of the latitudinal axis of convection over continental Asia from spring to autumn. Furthermore, the cold fronts that inject boundary layer air to the troposphere sweep down from the north (Siberia). It is possible that there is a local gradient in vertical transport over the Asian continent that opposes the gradient in radon source. This would account for the latitudinal gradient in radon concentration observed at Mauna Loa.

## 5. Conclusions

Results have been presented from hourly measurements of $^{222}$Rn in air parcels analysed at three ACE-Asia network sites in 2001. The location of the sites ensured that both the boundary layer and free tropospheric continental outflows were characterized simultaneously. Each site exhibited a unique seasonal cycle of radon concentration, for which the range of monthly mean concentrations was approximately 9520, 2410 and 160 mBq m$^{-3}$, for Hok Tsui, Gosan and Mauna Loa, respectively. Differences in amplitude and phase of the seasonal cycles between the sites was mainly attributed to (1) site location with respect to the Asian continental source, (2) dominant transport mechanisms and (3) regional/seasonal radon source variability. A pronounced seasonality in background radon concentration was characterized at each site, which provided a means by which to gauge the relative magnitude of continental influence on outflow events to the Pacific throughout the year. The background ratios of the summer minimum to the winter maximum were about 96, 15 and 3, for Hok Tsui, Gosan and Mauna Loa, respectively. Only in summer were background radon concentrations representative of typical marine baseline values ($\sim$20 mBq m$^{-3}$).

Ten-day back trajectories of air masses corresponding to high- and low-concentration radon events were used to characterize the seasonal variability in fetch regions of greatest and smallest terrestrial influence. Of the two coastal sites, fetch regions were more consistent at Hok Tsui than Gosan. A comparison of trajectories for high-radon events between these sites further supports claims of the presence of a large area with higher than average radon flux near the East China coast. However, there are insufficient data to determine whether this is a local phenomenon or represents part of a global latitudinal gradient postulated by other researchers. In any case, the magnitude of the observed difference in radon concentrations between Hok Tsui and Gosan indicates that the problem of radon flux heterogeneity is important at regional scales. Thus, unless the spatial heterogeneity of East Asian radon sources is taken into account within global/regional transport models, the quality of intercomparisons between modelled radon transport and observed radon time-series will be compromised. Likewise, some degree of the heterogeneity of regional radon sources in the vicinity of Hok Tsui will need to be accounted for if radon observations are to be used for trace gas inventory analyses in that region.

Back trajectories of tropospheric air masses reaching Mauna Loa indicate source regions deep within the Asian continent primarily between 20 and 40°N. This fetch region is quite distinct from that influencing the Hok Tsui and Gosan sites. The radon concentration of air masses reaching Mauna Loa was shown to vary seasonally, as well as with latitude of predominant fetch region. Possible mechanisms of this phenomenon were identified and included (1) seasonal variation in the radon source, (2) seasonal variation in the strength, frequency and/or efficiency of mechanisms that lift boundary layer air to the mid troposphere and (3) seasonal variation in the latitudinal axis of convection.

## 6. Acknowledgments

This research is a contribution to the International Global Atmospheric Chemistry (IGAC) Core Project of the International Geosphere Biosphere Program (IGBP) and is part of the IGAC Aerosol Characterization Experiments (ACE). The measurement activities at Hok Tsui were partly supported by the Background Air Monitoring Project of the Hong Kong Polytechnic University and by a grant (to T. Wang) from the Research Grants Council of Hong Kong (Project No. PolyU5063/01E). The measurement program at Gosan was partly supported by National Research Laboratory of METRI Korea. The authors would like to thank Mr Fukumura-Sawada of the Mauna Loa Observatory for his help in running the radon programme at the station. Mr Ot Sisoutham of the Australian Nuclear Science and Technology Organisation provided technical assistance for the project. The authors also wish to thank the anonymous reviewers for their constructive feedback.

## References

Akimoto, H., Mukai, H., Nishikawa, M., Murano, K., Hatakeyama, S. and co-authors. 1996. Long-range transport of ozone in the East Asian Pacific rim region. *J. Geophys. Res.* **101**(D1), 1999–2010.

Andreae, M. O., Berresheim, H., Andreae, T. W., Kritz, M. A., Bates, T. S. and co-authors. 1988. Vertical distribution of dimethylsulfide, sulfur dioxide, aerosol ions, and radon over the northeast Pacific Ocean. *J. Atmos. Chem.* **6**, 149–173.

Balkanski, Y. J., Jacob, D. J., Arimoto, R. and Kritz, M. A. 1992. Distribution of $^{222}$Rn over the North Pacific: implications for continental influences. *J. Atmos. Chem.* **14**, 353–374.

Board, A. S., Fuelberg, H. E., Gregory, G. L., Heikes, B. G., Schulz, M. G. et al., 1999. Chemical characteristics of air from differing source regions during the Pacific Exploratory Mission-Tropics A (PEM-Tropics A). *J. Geophys. Res.* **104**(D13), 16 181–16 196.

Bodhaine, B. A. 1983. Aerosol measurements at four background sites. *J. Geophys. Res.* **88**, 10 753–10 768.

Bodhaine, B. A. 1996. Aerosol measurements during the Mauna Loa Photochemistry Experiment 2. *J. Geophys. Res.* **101**(D9), 14 757–14 765.

Bodhaine, B. A., Mendonca, B. G., Harris, J. M. and Miller, J. M. 1981. Seasonal variations in aerosols and atmospheric transmission at Mauna Loa Observatory. *J. Geophys. Res.* **86**(C8), 7395–7398.

Climate Change, 2001. The Scientific Basis Contribution of Working Group I to the Third Assessment Report of the Intergovernmental Panel on Climate Change (IPCC). (eds J. T. Houghton, Y. Ding, D. J. Griggs, M. Noguer, P. J. van der Linden et al.). Cambridge University Press, Cambridge.

Conen, F. and Robertson, L. B. 2002. Latitudinal distribution of radon-222 flux from continents. *Tellus,* **54B**, 127–133.

Crawford, J., Davis, D., Chen, G., Bradshaw, J. D., Sandholm, S. T. et al. 1997. An assessment of ozone photochemistry in the extratropical western North Pacific: impact of continental outflow during the late winter/early spring. *J. Geophys. Res.* **102**(D23), 28 469–28 487.

Culf, A. D., Fisch, G., Malhi, Y. and Nobre, C. A. 1997. The influence of the atmospheric boundary layer on carbon dioxide concentrations over a tropical forest. *Agric. Forest. Meteorol.* **85**, 149–158.

Debaje, S. B., Vernekar, K. G. and Ramachandran, T. V. 1996. Study of atmospheric radon-222 concentrations at Pune. *Indian J. Environ. Prot.,* **16**(10), 755–760.

Dentener, F., Feichter, J. and Jeuken, A. 1999. Simulation of the transport of $^{222}$Rn using on-line and off-line global models at different horizontal resolutions: a detailed comparison with measurements. *Tellus,* **51B**, 573–602.

Dibb, J. E., Talbot, R. W., Klemm, K. I., Gregory, G. L., Singh, H. B. et al. 1996. Asian influence over the western North Pacific during the fall season: Inferences from $^{210}$Pb, soluble ionic species and ozone. *J. Geophys. Res.* **101**(D1), 1779–1792.

Dibb, J. E., Talbot, R. W., Lefer, B. L., Scheuer, E., Gregory, G. L. et al. 1997. Distributions of beryllium 7 and lead 210, and soluble aerosol-associated ionic species over the western Pacific PEM-West B, February–March 1994. *J. Geophys. Res.* **102**(D23), 28 287–28 302.

Dörr, H. and Münnich, K. O. 1990. $^{222}$Rn flux and soil air concentration profiles in West Germany. Soil $^{222}$Rn as a tracer for gas transport in the unsaturated soil zone. *Tellus* **42B**, 20–28.

Draxler, R. R. and Hess, G. D. 1997. Description of the HYSPLIT_4 modeling system. *NOAA Technical Memorandum ERL ARL-224 (revised 2004).* Air Resources Laboratory, Silver Spring, MD.

Draxler, R. R. and Hess, G. D. 1998. An overview of the HYSPLIT 4 modelling system for trajectories, dispersion and deposition. *Aust. Meteorol. Mag.* **47**, 295–308. (Further information regarding NOAA ARL's model HYSPLIT 4 is available from http://www.arl.noaa.gov/ready/hysplit4.html)

Gao, Y., Arimoto, R., Zhou, M. Y., Merrill, J. T. and Duce, R. A. 1992. Relationships between the dust concentrations over eastern Asia and the remote north Pacific. *J. Geophys. Res.* **97**(D9), 9867–9872.

Giannakopoulos, C., Chipperfield, M. P., Law, K. S., Plantevin, P.-H., Pyle, J. A. et al. 2000. A three-dimensional modelling study of the correlations of $^{210}$Pb with $HNO_3$ and peroxyacetylnitrate (PAN) at remote oceanic sites. *J. Geophys. Res.* **105**(D2), 1947–1956.

Giannakopoulos, C., Chipperfield, M. P., Law, K. S. and Pyle, J. A. 1999. Validation and intercomparison of wet and dry deposition schemes using $^{210}$Pb in a global three-dimensional off-line chemical transport model. *J. Geophys. Res.* **104**(D19), 23 761–23 784.

Gras, J. L. and Whittlestone, S. 1992. Radon and CN: complementary tracers of polluted air masses at coastal and island sites. *J. Radioanal. Nucl. Chem.* **161**(1), 293–306.

Gregory, G. L., Merrill, J. T., Shipham, M. C., Blake, D. R., Sachse, G. W. and co-authors. 1997. Chemical characteristics of tropospheric air over the Pacific Ocean as measured during PEM-West B: relationship to Asian outflow and trajectory history. *J. Geophys. Res.* **102**(D23), 28 275–28 285.

Guelle, W., Balkanski, Y. J., Dibb, J. E., Schulz, M. and Dulac, F. 1998a. Wet deposition in a global size-dependent aerosol transport model. 2. Influence of the scavenging scheme on $^{210}$Pb vertical profiles, surface concentrations, and deposition. *J. Geophys. Res.* **103**(D22), 28 875–28 891.

Guelle, W., Balkanski, Y. J., Schulz, M., Dulac, F. and Monfray, P. 1998b. Wet deposition in a global size-dependent aerosol transport model. 1. Comparison of a 1 year $^{210}$Pb simulation with ground measurements. *J. Geophys. Res.* **103**(D10), 11 429–11 445.

Harris, J. M. and Kahl, J. D. 1990. A descriptive atmospheric transport climatology for the Mauna Loa Observatory, using clustered trajectories. *J. Geophys. Res.* **95**(D9), 13 651–13 667.

Hattori, T. and Ichiji, T. 1998. Estimates of seasonal variations of $^{222}$Rn from different origins by using the correlation between $^{222}$Rn and $^{212}$Pb concentrations in air. In: *Radon and Thoron in the Human Environment* (eds A. Katase and M. Shimo). World Scientific Publishing, Singapore, 246–251.

Holmes, J. and Zoller, W. 1996. The elemental signature of transported Asian dust at Mauna Loa observatory. *Tellus* **48B**, 83–92.

Huebert, B. J., Bates, T., Russell, P. B., Shi, G., Kim, Y. J. et al., 2003. An overview of ACE-Asia: strategies for quantifying the relationships between Asian aerosols and their climatic impacts. *J. Geophys. Res.* **108**(D23), 8633–8633.

Iida, T., Yamada, K., Hashiguchi, Y., Moriizumi, J., Nagao, I. et al., 2000. Measurements of atmospheric radon concentrations at various locations in east Asia. In: *Distribution and Speciation of Radionuclides in the Environment* (edsJ. Inaba, S. Hisamatsu and Y. Ohtsuka). Rokkasho, Aomori, Japan, 123–132.

Jacob, D. J. and Prather, M. J. 1990. Radon-222 as a test of convective transport in a general circulation model. *Tellus* **42B**, 118–134.

Jacob, D. J., Prather, M. J., Rasch, P. J., Shia, R.-L., Balkanski, Y. J. et al., 1997. Evaluation and intercomparison of global atmospheric transport models using $^{222}$Rn and other short lived tracers. *J. Geophys. Res.* **102**(D5), 5953–5970.

Jaffe, D., Mahura, A., Kelley, J., Atkins, J., Novelli, P. C. et al. 1997. Impact of Asian emissions on the remote North Pacific atmosphere: Interpretation of CO data from Shemya, Guam, Midway and Mauna Loa. *J. Geophys. Res.* **102**(D23), 28 627–28 635.

Jin, Y., Iida, T., Ikebe, Y., Wang, Z. and Abe, S. 1998. A sub-nationwide survey of outdoor and indoor $^{222}$Rn concentrations in China by passive method. In: *Radon and Thoron in the Human Environment* (eds A. Katase and M. Shimo). World Scientific Publishing, Singapore, 246–251.

Johnson, J. 2001. *Atmospheric Chemistry data from R/V Ronald H. Brown during the ACE-Asia IOP, 2001*, http://saga.pmel.noaa.gov/aceasia/rhb_data/index.html.

Kajii, Y., Akimoto, H., Komazaki, Y., Tanaka, S., Mukai, H. et al. 1997. Long-range transport of ozone, carbon monoxide, and acidic trace gases at Oki Island, Japan, during PEM-West B/PEACAMPOT B campaign. *J. Geophys. Res.* **102**(D23), 28 637–28 649.

Kritz, M. A. 1990. The China Clipper—fast advective transport of radon-rich air from the Asian boundary layer to the upper troposphere near California. *Tellus* **42B**, 46–61.

Kritz, M. A., Rosner, S. W., Kelly, K. K., Loewenstein, M. and Chan, K. R. 1993. Radon measurements in the lower tropical stratosphere: evidence for rapid vertical transport and dehydration of tropospheric air. *J. Geophys. Res.* **98**(D5), 8725–8736.

Lambert, G., Polian, G., Sanak, J., Ardouin, B., Buisson, A. and co-authors. 1982. Cycle du radon et de ses descendants: applicationàl'étude deséchanges troposphère-stratosphère. *Ann. Géophys*. **38**, 497–531.

Lambert, G., Polian, G. and Taupin, D. 1970. Existence of periodicity in radon concentrations and in the large scale distribution at lower altitudes between 40° and 70°S. *J. Geophys. Res.* **75**, 2341–2345.

Larson, R. E. and Hoppel, W. A. 1973. Radon 222 measurements below 4 km as related to atmospheric convection. *Pure Appl. Geophys.* **105**, 900–906.

Lee, H. N. and Feichter, J. 1995. An intercomparison of wet precipitation scavenging schemes and emission rates of $^{222}$Rn for the simulation of global transport and deposition of $^{210}$Pb. *J. Geophys. Res.* **100**(D11), 23 253–23 270.

Li, Y. and Chang, J. 1996. A three-dimensional global episodic tracer transport model. 1: Evaluation of its transport processes by radon 222 simulations. *J. Geophys. Res.* **101**, 25 931–25 947.

Littmann, T. 1991. Dust storm frequency in Asia: climatic control and variability. *Int. J. Climatol.* **11**, 393–412.

Liu, T. S. 1985. *Loess and the Environment*. China Ocean Press, Beijing, 215.

Martin, B. D., Fuelberg, H. E., Blake, N. J., Crawford, J. H., Logan, J. A. and co-authors. 2003. Long-range transport of Asian outflow to the equatorial Pacific. *J. Geophys. Res.* **108**(D2), 8322 doi: 10.1029/2001JD001418, 2002. [printed 108(D2), 2003].

Mendonca, B. G. 1969. Local wind circulation on the slopes of Mauna Loa. *J. Appl. Meteorol.* **8**, 533–541.

Merrill, J. T. 1990. Atmospheric long range transport to the Pacific Ocean. *Chem. Oceanogr.* **10**, 15–49.

Merrill, J. T. 1996. Trajectory results and interpretation for PEM-West A. *J. Geophys. Res.* **101**(D1), 1679–1690.

Merrill, J. T., Uematsu, M. and Bleck, R. 1989. Meteorological analysis of long range transport of mineral aerosols over the North Pacific. *J. Geophys. Res.* **94**(D6), 8584–8598.

Nakaya, U., Sugaya, J. and Shoda, M. 1957. Report of the Mauna Loa expedition in the winter of 1956–57. *J. Fac. Sci. Ser.1-7, Hokkaido Univ.*, **5**, 1–36.

Perry, K. D., Cahill, T. A., Schnell, R. C. and Harris, J. M. 1999. Long-range transport of anthropogenic aerosols to the National Oceanic and Atmospheric Administration baseline station at Mauna Loa Observatory, Hawaii. *J. Geophys. Res.* **104**(D15), 18 521–18 533.

Pochanart, P., Hirokawa, J., Kajii, Y. and Akimoto, H. 1999. Influence of regional-scale anthropogenic activity in northeast Asia on seasonal variations of surface ozone and carbon monoxide observed at Oki, Japan. *J. Geophys. Res.* **104**(D3), 3621–3631.

Schery, S. D. and Wasiolek, M. A. 1998. Modeling radon flux from the earth's surface. In: *Radon and Thoron in the Human Environment* (eds A. Katase and M. Shimo). World Scientific Publishing, Singapore, 207–217.

Schery, S. D., Whittlestone, S., Hart, K. P. and Hill, S. E. 1989. The flux of radon and thoron from Australian soils. *J. Geophys. Res.* **94**, 8567–8576.

Talbot, R.W., Dibb, J. E., Lefer, B. L., Bradshaw, J. D., Sandholm, S. T. and co-authors. 1997. Chemical characteristics of continental outflow from Asia to the troposphere over the western Pacific Ocean during February–March 1994: results from PEM-West B. *J. Geophys. Res.* **102**(D23), 28 255–28 274.

Thomas, J. W. and LeClare, P. C. 1970. A study of the two-filter method for radon-222. *Health Phys.* **18**, 113–122.

Turekian, K. K., Nozaki, Y. and Benninger, L. K. 1977. Geochemistry of atmospheric radon and radon products. *Ann. Rev. Earth Planet. Sci.* **5**, 227–255.

Ussler, W., Chanton, J. P., Kelly, C. A. and Martens, C. S. 1994. Radon-222 tracing of soil and forest canopy trace gas exchange in an open canopy forest. *J. Geophys. Res.* **99**, 1953–1963.

Wang, T., Lam, K. S., Chan, L. Y., Carroll, M. A. and Lee, A. S. Y. 1997. Trace gas measurements in coastal Hong Kong during the PEM-WEST (B). *J. Geophys. Res.* **102**, 28 575–28 588.

Wang, T., Ding, A. J., Blake, D. R., Zahorowski, W., Poon, C. N. and Li, Y. S. 2003. Chemical characterization of the boundary layer outflow of air pollution to Hong Kong during February-April 2001. *J. Geophys. Res.* **108**, D20 8787–8801, doi:10.1029/2002JD003272.

Whittlestone, S. and Zahorowski, W. 1998. Baseline radon detectors for shipboard use: development and deployment in the first Aerosol Characterisation Experiment (ACE 1). *J. Geophys. Res.* **103**, 16 743–16 751.

Wilkening, M. H. and Clements, W. E. 1975. Radon 222 from the ocean surface. *J. Geophys. Res.* **80**, 3828–3830.

Xu, N., Wei, F. S., Ten, E. J. and Chen, L. Q. 1993. Evaluation of indigenous concentrations of uranium and thorium in soils of China. *Commun. Soil Sci. Plant Anal.*, **24**, 1795–1803.

Yamanishi, H., Iida, T., Ikebe, Y., Abe, S. and Hata, T. 1991. Measurements of regional distribution of radon-222 concentration. *J. Nucl. Sci. Tech. Tokyo,* **28**(4), 331–338.

Zahorowski, W. and Whittlestone, S. 1999. Radon database 1987–1996: a review. In: *Baseline Atmospheric Program (Australia) 1996,* (eds J. L. Gras, N. Derek, N. W. Tindale and A. L. Dick). Bureau of Meteorology and CSIRO Atmospheric Research, Melbourne, 71–80.

Zhang, D. E. 1984. Synoptic-climate studies of dust fall in China since historic times. *Zhongguo Kexue Bji* **XXVII**, 825–836.